NANOSYSTEMS:
PHYSICS, CHEMISTRY, MATHEMATICS

Konovalova V.P., et al. *Nanosystems: Phys. Chem. Math.*, 2026, **17** (1), 69–80.
http://nanojournal.ifmo.ru
DOI 10.17586/2220-8054-2026-17-1-69-80

Original article

In situ XRD study of the crystallization process of MnO_x–ZrO_2 oxide

Valeria P. Konovalova[1], Evgeny Yu. Gerasimov[1], Zahar S. Vinokurov[2], Alena A. Pochtar[1], Olga A. Bulavchenko[1,2]

[1]Boreskov Institute of Catalysis SB RAS, Novosibirsk, Russia

[2]Synchrotron Radiation Facility SKIF, Kol'tsovo, Russia

Corresponding author: Valeria P. Konovalova, lekorux@gmail.com

PACS 82.33.Pt

ABSTRACT The crystallization process of MnO_x–ZrO_2 mixed oxide in different gas environments was studied by in situ X-ray diffraction and thermogravimetric analysis. The non-modified ZrO_2 was used as a reference. The process of crystallization in Mn-containing sample dependents on the environment: the crystallization temperature in reducing and inert environment was 450 – 455 °C and in oxidizing it was 560 °C. Thus, the addition of manganese led to the shift of crystallization temperature to the higher values compared to reference sample ZrO_2 (425 °C). The resulting crystalline phase was $Zr_{1-y}Mn_yO_2$ solid solution rather than pure zirconia. Mn cations seemed to stabilize the tetragonal zirconia instead of monoclinic.

KEYWORDS in situ XRD, crystallization, manganese oxide, solid solution, zirconia

ACKNOWLEDGEMENTS The work was supported by the Ministry of Science and Higher Education of the Russian Federation within the governmental order for Boreskov Institute of Catalysis (project FWUR-2024-0032).

FOR CITATION Konovalova V.P., Gerasimov E.Yu., Vinokurov Z.S., Pochtar A.A., Bulavchenko O.A. In situ XRD study of the crystallization process of MnO_x–ZrO_2 oxide. *Nanosystems: Phys. Chem. Math.*, 2026, **17** (1), 69–80.

1. Introduction

Zirconia-based materials are applied for different practical purposes: as refractory materials, pigments, piezoelectric devices, ceramic capacitors, oxygen sensors, etc. These materials are also used as catalysts and supports [1] for WGS reaction [2], reduction of CO, NO_x and volatile organic compounds (VOC) [3], alkane isomerization reactions [4, 5] etc.

Zirconia has three stable modifications: monoclinic (m-ZrO_2), tetragonal (t-ZrO_2) and cubic (c-ZrO_2). Monoclinic modification is stable at room temperature, tetragonal at temperatures of 1170 – 2370 °C and cubic above 2370 °C [6]. One of the ways to obtain solid crystalline form of zirconia phase is the calcination of amorphous precursor. During calcination, crystallization occurs with the formation of various modifications of ZrO_2 or their mixture. The crystalline phase (or phases) directly depends on the state of the original amorphous compound, thus, understanding the nature of the amorphous precursor and the process of its crystallization is important to unravel the structure and, consequently, the properties of the resulting crystalline materials.

The pathway of phase transformations during the crystallization of an amorphous precursor is directly influenced by local structure of initial compound. This is because the local structure reflects the state of the crystalline grains. Yanwei et al. [7] described a local structure of amorphous phase as monoclinic-like in xerogel and aerogel synthesized ZrO_2 samples. Crystallization took place at the temperature of 400 °C with the formation of monoclinic ZrO_2 crystallites. Tiseanu et al. [8] found crystallographic planes typical for m-ZrO_2 and t-ZrO_2 in amorphous sample synthesized by oil-in-water method. Temperature-induced crystallization has resulted in the formation of crystalline tetragonal zirconia at 450 °C.

Both the crystallization temperature and the resulting phases depend on the state of the amorphous precursor. The introduction of dopant atoms also has a significant effect on the crystallization process. For example, the authors [9, 10] showed that the introduction of vanadium into amorphous ZrO_2 leads to an increase in the crystallization temperature. Ushakov et al. [11] showed a similar effect during doping with lanthanum and yttrium. In all these works, it was shown that doping of amorphous zirconia can lead to the preferential formation of thermodynamically metastable tetragonal and/or cubic modification of zirconia instead of monoclinic.

To the best of our knowledge, there are no works that would consider the crystallization process of amorphous zirconium doped with Mn. However, the addition of manganese can have a crucial effect on the catalytic properties [12–16]. Catalytic activity in oxidation reactions of manganese oxides is associated with the variety of oxidation states of manganese and due to the ability of manganese ions to easily change their oxidation state [17]. In MnO_x–ZrO_2 mixed oxide catalysts, various active states can be formed depending on the synthesis conditions. For example, wet impregnation of zirconia with a manganese nitrate solution results in the formation of nanoparticles of α-Mn_2O_3 supported on ZrO_2. By coprecipitation of metal acetates and nitrates, $Mn_xZr_{1-x}O_2$ solid solution is obtained [15, 18, 19]. Previously [20] we

succeeded in synthesizing the amorphous phase by coprecipitation of manganese and zirconium nitrates. This amorphous phase itself had low catalytic activity, but calcination at higher temperatures led to the formation of a highly active $Mn_xZr_{1-x}O_2$ solid solution and in the tetragonal/cubic modification. Therefore, on the one hand, it is important to study the crystallization process as a path to the formation of a solid solution, and on the other hand, the investigation of the amorphous precursor can shed light on the influence of dopant atoms on this process. In this work we focused on determining the crystallization mechanism of amorphous MnO_x–ZrO_2 oxide catalyst depending on the gas atmosphere. Conventional X-ray diffraction (XRD) analysis is not suitable for studying amorphous compounds due to the lack of long-range order. Instead, better approach is to determine their local structure using pair distribution function analysis (PDF). In order to investigate temperature-induced phase transformations and structural changes in different environments in situ X-ray diffraction technique and thermogravimetric analysis (TGA) were applied. Morphology of the investigated samples was studied via transmission electron microscopy (TEM) and BET technique.

2. Experimental

2.1. Catalyst preparation

Catalysts with the ratio Mn/Zr = 1/4 were synthesized by co-precipitation of a joint solution of $ZrO(NO_3)_2$ and $Mn(NO_3)_2$ salts by the dropwise addition of NH_3(aq) and vigorous stirring until pH 10 was reached. The resulting precipitate was filtered, washed with water to pH 6 – 7 and dried at 120 °C, and then calcined at a given temperature for 4 h at the temperatures 400 and 700 °C. The catalysts obtained were designated as Mn–Zr–T, where T is the calcination temperature. The reference sample containing no manganese admixture was synthesized by similar precipitation of zirconium nitrate and calcined at 300 °C for 4 hours. This sample was designated as ZrO_2-300.

2.2. Ex situ & in situ X-ray diffraction (XRD)

The XRD patterns were obtained via diffractometer STOE STADI MP (Germany) in the 2θ range from 10 to 50° with a step of 0.015° and an accumulation time of 70 s per point. MoKα radiation with wavelength $\lambda = 0.7093$ Å was applied. In situ XRD studies were carried out on a High Precision Diffractometry II station (The Siberian Synchrotron and Terahertz Radiation Centre, Novosibirsk, Russia). The X-ray diffractometer at the station included a monochromator, a collimation system, and an OD-3M single-coordinate position-sensitive detector [21]. The working radiation wavelength ($\lambda = 1.6467$ Å) was set by a single reflection from a Ge (111) crystal monochromator. The diffractometer is equipped with a high-temperature reactor XRK-900 (Anton Paar, Austria). A quadrupole mass spectrometer (SRS UGA100, USA) was used to control the gas environment. Heating was carried out at a constant rate of 10 °/min, the gas mixture feed rate was 100 ml/min. The ICDD PDF-2 powder database was used for phase analysis [22]. Quantitative phase analysis and refinement of the lattice parameters were performed by the Rietveld method using the XPert HighScore Plus software [23]. CSR were calculated via Sherrer equation [24]. Corundum was used to subtract the instrumental broadening.

In order to compare the lattice parameters of cubic and tetragonal zirconia phases, we used the normalized lattice parameter a^* in the case of tetragonal oxide:

$$a^* = \left(\frac{V_{\text{tetr}} \cdot Z_{\text{cub}}}{Z_{\text{tetr}}}\right)^{1/3},$$

where $V_{\text{tetr}} = a^2 \cdot c$ is the volume of a tetragonal cell, $Z_{\text{cub}} = 4$, $Z_{\text{tetr}} = 2$ is the number of units in the cubic and tetragonal cells, respectively.

2.3. Pair Distribution Function analysis (PDF)

The diffraction pattern for PDF analysis was recorded using a laboratory diffractometer STOE STADI MP (Germany) with MoKα radiation ($\lambda = 0.7093$ Å) in the range of 2θ from 1.5 to 126.9° with a step of 0.015° for 200 s at each point. The relationship between the distribution function of atomic pairs G(r) and coherent scattering of X-rays is determined through the Fourier transform:

$$G(r) = \frac{2}{\pi} \int_0^\infty Q \cdot i(Q) \cdot \sin(Qr) \cdot dQ.$$

To obtain pair distribution functions from X-ray diffraction data by Fourier transform we used PDFgetX2 [25]. The obtained PDF data were then analyzed using PDFgui software [26].

2.4. Thermogravimetric analysis (TGA)

Thermogravimetric analysis of Mn–Zr-400 and ZrO_2 samples was carried out using STA 449 C Jupiter synchronous thermal analysis device from NETZSCH (Germany). A sample portion (45.14 mg) was placed in a corundum crucible. The sample was heated in an air and helium atmosphere from the room temperature to 900 °C with a heating rate of 5 °C/min and a gas feed rate of 30 ml/min. The experimental data were analyzed using the NETZSCH Proteus Thermal Analysis software package.

2.5. Transmission electron microscopy (TEM)

The morphology and microstructure of the samples were studied by transmission electron microscopy. TEM images were obtained on a ThemisZ Thermo Fisher Scientific microscope (Thermo Fisher Scientific, Eindhoven, The Netherlands) with a resolution of 0.7 Å. EDX analysis was carried out on an energy dispersive spectrometer SuperX (Thermo Fisher Scientific). Samples for research were fixed on standard copper grids using ultrasonic dispersion of the catalysts in ethanol.

The specific surface area was calculated with the Brunauer–Emmett–Teller (BET) method using nitrogen adsorption isotherms measured at liquid nitrogen temperatures on QuadraSorb SI MP Station (Micromeritics Instrument Corp., Norcross, GA, USA).

3. Results

3.1. XRD analysis

The diffraction patterns of double oxides Mn–Zr-400, Mn–Zr-700 and reference sample ZrO_2-300 are shown in Fig. 1. The sample Mn–Zr-700 is presented by the diffraction maxima at 2θ = 13.9, 15.8, 16.1, 19.6, 22.6, 22.8, 26.5, 26.8, 27.9, 32.1, 32.5, 35.3, 35.5, 36.18, 40.0, 41.5 and 42.6°, which correspond to the peaks hkl = 011, 002, 110, 012, 112, 020, 013, 121, 022, 004, 220, 123, 031, 114, 132, 124 and 231 of the t-ZrO_2 phase (s.g. P 4_2/nmc, PDF 50-1089). The Rietveld refinement showed the lattice parameters $a = b = 3.606(1)$ Å and $c = 5.078(1)$ Å that corresponds the normalized lattice parameter $a^* = 5.090(1)$ Å. The lattice parameter for pure c-ZrO_2 is 5.11 Å [27], which indicates the formation of the $Zr_{1-y}Mn_yO_2$ solid solution phase due to the ionic radius of Mn (Mn^{3+} – 0.66 Å) being smaller than the ionic radius of Zr (Zr^{4+} – 0.79 Å) [28].

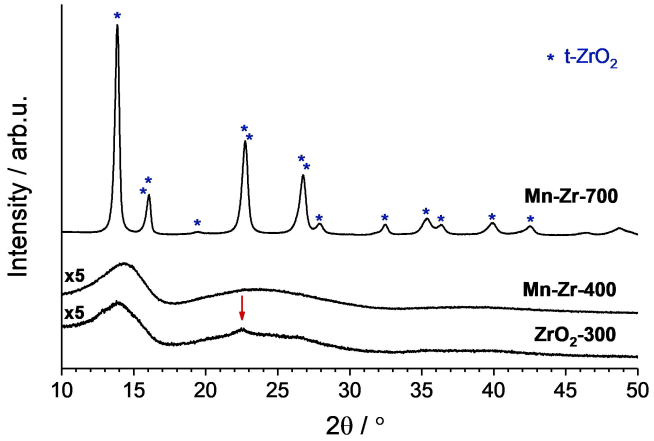

FIG. 1. XRD patterns of ZrO_2-300, Mn–Zr-400 and Mn–Zr-700; $\lambda = 0.7093$ Å.

The diffraction patterns of Mn–Zr-400 and ZrO_2-300 samples contain broad diffraction maxima typical for amorphous state. The XRD pattern of ZrO_2 also has a small narrow diffraction peak at 2θ = 22.4°, which probably indicates partial formation of a crystalline phase. This peak does not belong to any specific phase, but according to the literature on zirconium modifications, the formation of m-ZrO_2 is most likely at this temperature [6]. However, the sample Mn–Zr-400 does not contain any narrow peaks other than broad amorphous ones. Moreover, there is a significant difference in the specific surface area (S_{BET}) which is shown in Table 1. It can be seen that S_{BET} of Mn–Zr-400 sample is 331 m^2/g, which is three times larger than that of ZrO_2 sample (108 m^2/g). Usually, the specific surface area decreases with the increase in the calcination temperature, but we see an inverse relationship, indicating that the Mn presence in Mn–Zr-400 sample contributes to a significant increase in the specific surface area. The S_{BET} of the sample Mn–Zr-700 is only 38 m^2/g, which is expected given the increase in calcination temperature up to 700 °C.

It is known that heating of pure amorphous ZrO_2 leads to the formation of monoclinic [7] or a mixture of monoclinic and tetragonal zirconia [8,29]. In the case of Mn doping, only the tetragonal modification is formed. This is probably due to the stabilization by introducing manganese. In addition, the presence of manganese apparently delays the crystallization process, since the Mn–Zr-400 sample does not show any narrow peaks corresponding to the crystalline phase.

3.2. TEM and EDX analysis

TEM images of Mn–Zr-400 show the presence of large amorphous aggregates of about 200 – 400 nm in size (Fig. 2a) and long cylindrical particles about 150 – 200 nm long and 10 – 30 nm wide (Fig. 2b). The large particles are an amorphous state containing no crystalline planes (Fig. 2c). According to the EDX analysis (Fig. 2d, area 1), in these regions Zr and

TABLE 1. Structural characteristics of the samples

Sample	Phase composition, wt. %	CSR, Å	Normalized lattice parameter, Å	S_{BET}, m^2/g
ZrO_2-300	amorphous	—	—	108
Mn–Zr-400	amorphous	—	—	331
Mn–Zr-700	t-ZrO_2*	100	5.090(1)	38

* $Zr_{1-y}Mn_yO_2$ solid solution

Mn atoms have a uniform distribution with a ratio Mn/Zr = 0.22. The cylindrical particles contain only Mn atoms which is shown by the EDX analysis (Fig. 2d, area 2), and these particles have visible crystalline planes (Fig. 2c) corresponding to the Mn_3O_4 phase (s.g. I 4_1/amd, PDF 240734).

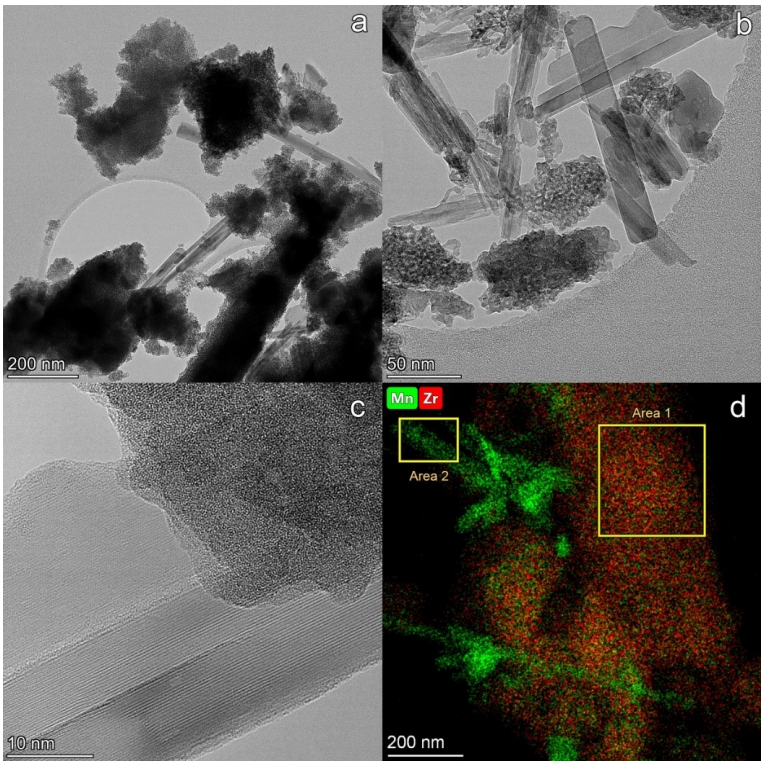

FIG. 2. TEM images (a, b, c) and EDX mapping (d) of Mn–Zr-400

In Fig. 3 TEM images of Mn–Zr-700 sample are shown. It can be seen that the sample contains crystalline particles of 20 – 30 nm in size combined together into large aggregates of about 500 nm and bigger. According to the EDX analysis (Fig. 3c, Area 1), the distribution of Zr and Mn atoms in the sample is mostly uniform. Mn/Zr atomic ratio is approximately 0.22, as in the amorphous sample Mn–Zr-400. Unlike the Mn–Zr-400 sample, the crystalline planes are detected in the particles, so the formation of crystalline $Zr_{1-y}Mn_yO_2$ solid solution is observed, that matches the XRD data. However, this sample also contains areas with higher manganese content (Fig. 3d, Area 3), which also indicates the presence of a separate manganese oxide phase.

TEM images of ZrO_2-300 are shown in Fig. 4. This sample mainly consists of amorphous particles (Fig. 4b) forming layered large aggregates (Fig. 4a). However, there are also few regions containing crystalline planes (Fig. 4b, Area 1). This result also correlates with the XRD data, which showed the presence of small peaks corresponding to crystalline zirconia unlike the sample Mn–Zr-400.

Thus, the results of TEM and EDX analysis indicate the formation of particles with uniform distribution of Mn and Zr atoms in the Mn–Zr-400 and Mn–Zr-700 samples. The atomic ratio of Mn/Zr in both remains approximately 0.22. So, we can conclude the formation of $Zr_{1-y}Mn_yO_2$ solid solution in both samples, but it is amorphous in the sample Mn–Zr-400. Also, both samples show the formation of manganese oxide phase, despite the Mn–Zr atomic distribution is

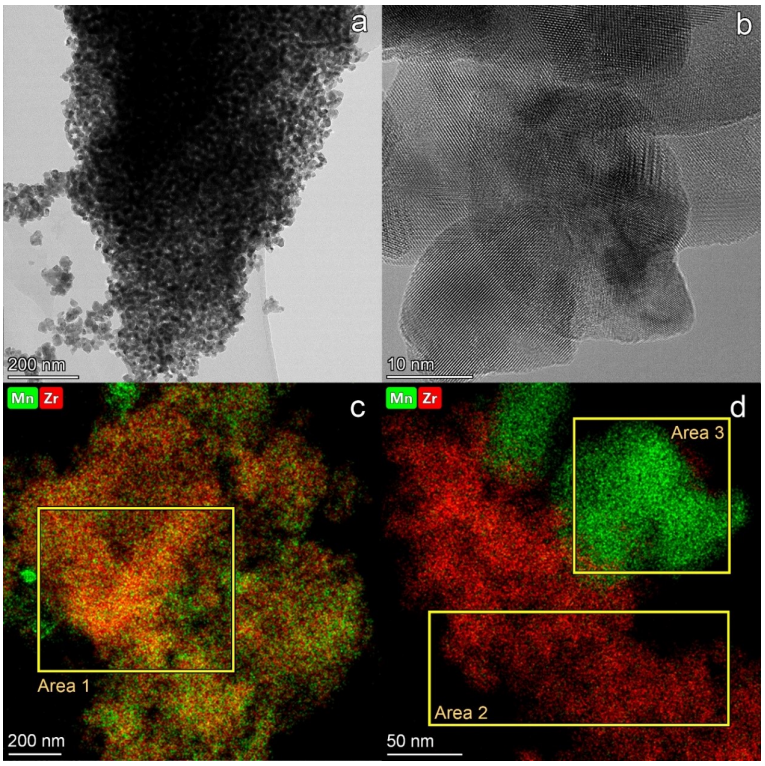

FIG. 3. TEM images (a, b) and EDX mapping (c, d) of Mn–Zr-700

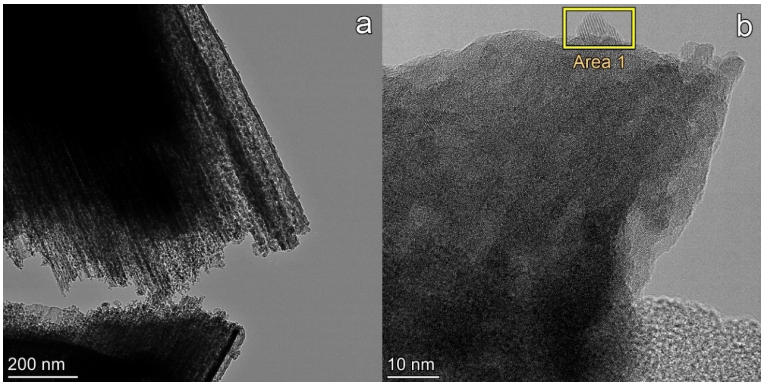

FIG. 4. TEM images (a, b) of ZrO_2-300

mostly uniform. The detected crystalline particles of Mn_3O_4 probably cannot be detected by XRD due to their disorder, planar defects, and small amount relative to the solid solution phase.

3.3. PDF analysis

The catalysts Mn–Zr-400 and Mn–Zr-700 were investigated by the PDF analysis, and ZrO_2-300 was used as a reference sample. Fig. 5a shows the $G(r)$ functions for these samples. It is seen that the PDFs of low-temperature oxides Mn–Zr-400 and ZrO_2-300 fall off at about 10 Å, indicating the typical for amorphous state absence of long-range order. These particles can be considered as crystalline nuclei, which form the bulk crystalline phase ZrO_2 with increasing temperature [7]. On the contrary, the Mn–Zr-700 sample, has the typical PDF for a crystalline compound – the amplitude of the $G(r)$ peaks does not decrease at large r. Nevertheless, a comparison of these PDFs is possible within the first few coordination spheres.

In the case of Mn-containing oxides, the first coordination distance Zr–O is about 2.12 – 2.14 Å, whereas for the ZrO_2-300 sample it is about 2.20 Å. This difference is probably due to the presence of the MnO_x phase, which was detected by TEM. However, at large distances, there is more similarity between the Mn–Zr-700 and ZrO_2-300 samples than between Mn–Zr-700 and Mn–Zr-400. This is probably due to the fact that ZrO_2-300, according to the XRD data, contains some crystalline ZrO_2 phase.

To estimate the contribution of the added manganese, the $G(r)$ function of ZrO_2-300 was subtracted from the $G(r)$ of Mn–Zr-400. The residual $G(r)$ is shown in Fig. 5b. The Mn–O distance is about 2.01 Å, that is close to the distance 2.02 Å corresponding both Mn_2O_3 (s.g. Ia-3, COD 1514107) and Mn_3O_4 (s.g. I 4_1/amd, COD 1011262). Mn–Mn distances of the nearest coordination spheres are in the r range of 2.84 – 4.22 Å, that are close to those of the oxides Mn_2O_3 (2.86 – 4.24 Å) and Mn_3O_4 (2.80 – 4.23 Å). However, according to TEM data, this phase is most likely to represent Mn_3O_4. Thus, the residual $G(r)$ function is likely to represent manganese oxide phase in the sample Mn–Zr-400.

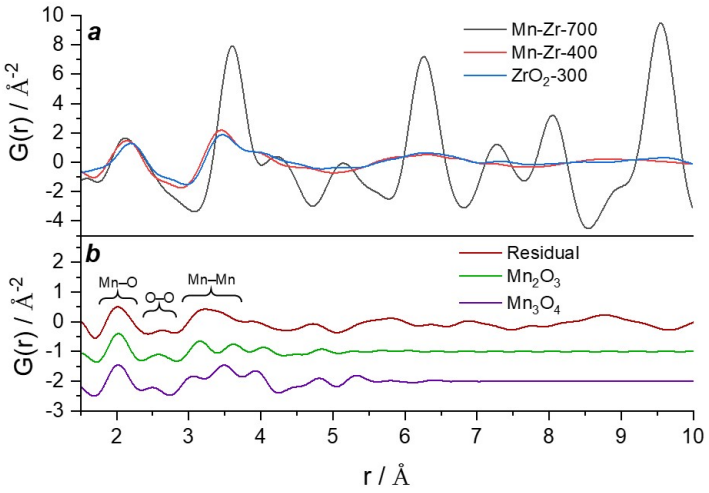

FIG. 5. Comparison of $G(r)$ functions of Mn–Zr-700, Mn–Zr-400 and ZrO_2-300 (a); residual $G(r)$ of Mn–Zr-400 and ZrO_2-300 (b)

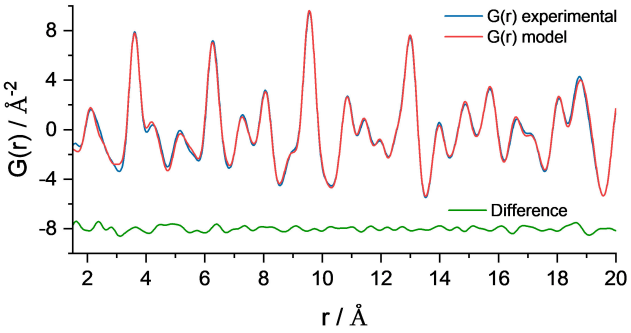

FIG. 6. Experimental and calculated (P 4_2/nmc, $Zr_{0.89}Mn_{0.11}O_{1.88}$) functions $G(r)$ of the sample Mn–Zr-700

Figure 6 shows the experimental and calculated functions $G(r)$ for the Mn–Zr-700 sample. All coordination peaks of this function correspond to the distances typical for the fluorite structure. According to the XRD data, calculated $G(r)$ function should contain $Zr_yMn_{1-y}O_2$ solid solution phase based on t-ZrO_2 structure. The normalized lattice parameter a^* is 5.099(1) Å is close to Rietveld refined one. Refinement model contains the atomic ratio Mn/Zr in solid solution phase 0.11/0.89 and the oxygen occupancy 0.94. It also should be mentioned that, according to the TEM data, this sample contains the MnO_x phase. Probably, some discrepancy between the experiment and simulation is due to the contribution of this phase.

3.4. In situ XRD

To establish the peculiarities of the crystallization process depending on the temperature and gas environment, in situ XRD experiment was carried out for the sample Mn–Zr-400. The catalyst was heated to 700 °C in inert (He), reducing (H_2/He, 10/90 sccm) and oxidizing (O_2/He, 20/80 sccm) environments at a rate of 5°C /min.

The diffraction patterns obtained by heating Mn–Zr-400 in He are shown in Fig. 7a. At room temperature, a broad halo is observed, indicating an amorphous state. The crystallization process begins at 455 °C, small peaks of the crystalline phase appear. The resulting crystalline phase is cubic ZrO_2 (s.g. Fm-3m, PDF 77-2157) which is represented by diffraction

maxima at 32.6 and 37.8 °2θ corresponding to reflections 111 and 200, respectively. During heating, intensity of these peaks gradually increases along with the disappearance of the amorphous phase that indicates crystallization of solid solution.

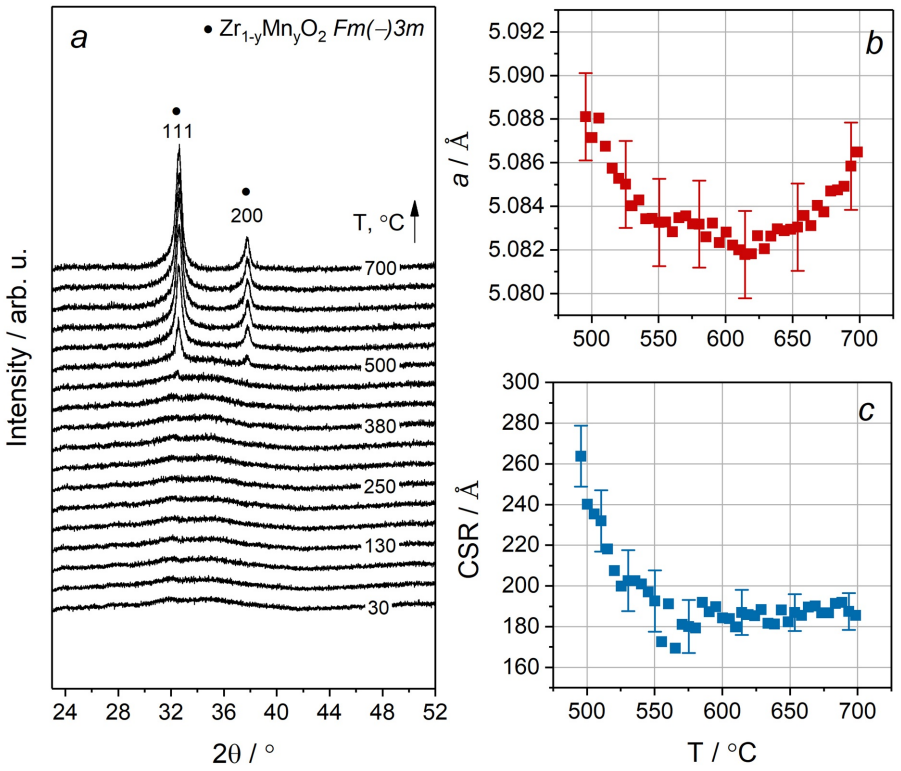

FIG. 7. XRD patterns of Mn–Zr-400 recorded upon heating from 30 to 700 °C with a rate of 5 °C/min in the He medium; $\lambda = 1.6467$ Å (a) change in the lattice parameter (b) and CSR (c) of $Zr_{1-y}Mn_yO_2$ with temperature

The lattice parameter of the crystalline phase at 500 °C is 5.088(2) Å. Despite the thermal expansion of the lattice, this value is lower than for pure ZrO_2 (5.11 Å), which indicates the formation of the $Zr_{1-y}Mn_yO_2$ solid solution phase instead of pure zirconia. During further heating, the lattice parameter decreases even more (Fig. 7b), reaching a minimum value 5.082(2) Å at 600 – 650 °C. The continuous nature of this process indicates that the formation of the solid solution phase is gradual. Mn cations probably migrate from the Mn_3O_4 oxide phase detected by TEM and / or from the remaining amorphous precursor and slowly substitute Zr cations. So, at the temperatures of 600 – 650 °C, the highest concentration of manganese is achieved in $Zr_{1-y}Mn_yO_2$. At the same time, the CSR value of $Zr_{1-y}Mn_yO_2$ decreases from 260 to 180 Å (Fig. 7c). After reaching the minimum value at 600 – 650 °C, the lattice parameter increases with temperature reaching the maximum value 5.086(2) Å at 700 °C. However, CSR of phase $Zr_{1-y}Mn_yO_2$ is generally stable upon further heating. Besides thermal expansion, the parameter growth may indicate two processes: the reduction of Mn cations in the solid solution or the decomposition of the solid solution with the release of manganese. In the first case, the parameter growth is due to the fact that the ionic radius of Mn cations is inversely proportional to their oxidation state [28]. In the second case, manganese atoms are released from the solid solution lattice with formation of MnO_x oxide.

In the reducing environment (H_2/He), the crystallization process occurs similarly (Fig. A1 in Appendix). The diffraction maxima of the $Zr_{1-y}Mn_yO_2$ solid solution phase appear at 450 °C indicating the beginning of the crystallization process. The lattice parameter of $Zr_{1-y}Mn_yO_2$ is about 5.088(2) Å, and it gradually decreases with heating to the minimum value 5.075(2) Å at the temperature about 550 – 600 °C. Simultaneously, there is a decrease in the CSR value from the initial 290 to 190 Å. Further heating leads to an increase in the lattice parameter of $Zr_{1-y}Mn_yO_2$ up to 5.083(2) Å at 700 °C, while CSR is stable. Therefore, we can conclude that the reducing environment has no significant effect on the crystallization process of the $Zr_{1-y}Mn_yO_2$ solid solution phase compared to an inert environment.

In the oxidizing environment (O_2/He), the XRD peaks of the crystalline phase $Zr_{1-y}Mn_yO_2$ appear at the temperature 560 °C (Fig. 8a), which means that the crystallization process begins at a higher temperature than in inert and reducing environments. The lattice parameter of $Zr_{1-y}Mn_yO_2$ also decreases with increasing temperature from initial 5.086(2) Å to its minimum value 5.072(2) Å at 660 – 700 °C (Fig. 8b). The CSR value at the beginning of the crystallization process is lower than in reducing and inert environments (200 Å), but also steadily decreases to 120 Å upon heating (Fig. 8c).

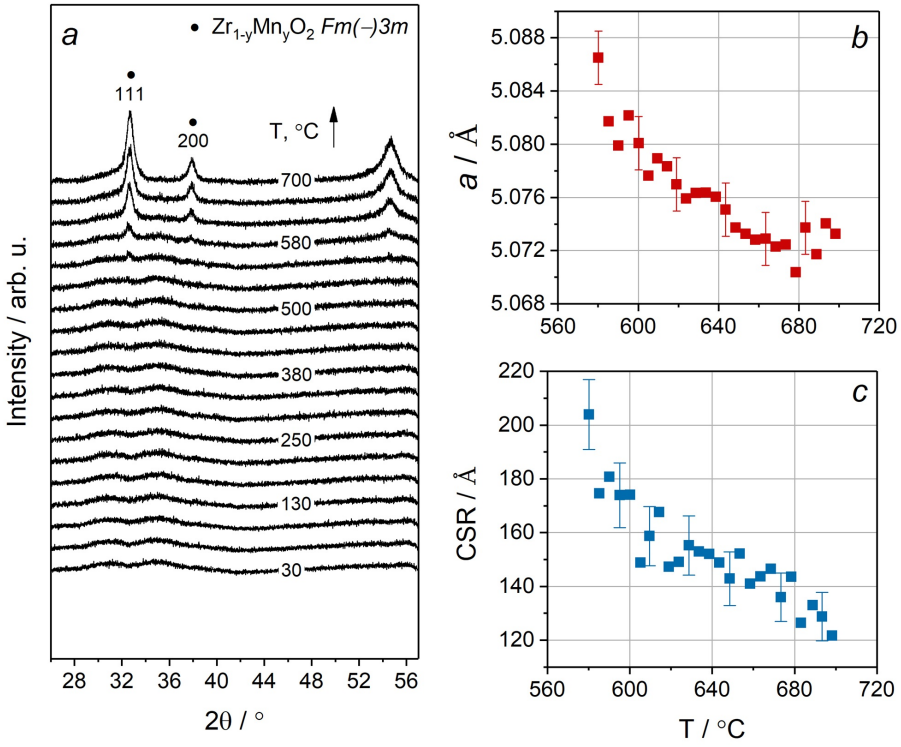

FIG. 8. XRD patterns of Mn–Zr-400 recorded upon heating from 30 to 700 °C with a rate of 5 °C/min in the O_2/He medium; $\lambda = 1.6467$ Å (a) change in the lattice parameter (b) and CSR (c) of $Zr_{1-y}Mn_yO_2$ with temperature

Table 2 shows the properties of the Mn–Zr-400 catalyst after in situ XRD experiments carried out in the corresponding environments. The $Zr_{1-y}Mn_yO_2$ solid solution phase is obviously preserved, as indicated by the lattice parameter value being in the range 5.055(1) – 5.065(1) Å. It was shown that the effect of an oxidizing environment led to the formation of a solid solution with the lowest lattice parameter (5.055(1) Å).

TABLE 2. Phase composition, CSR and lattice parameter in Mn–Zr-400 oxide after the in situ XRD experiments

Medium	Phase composition, wt. %	CSR ($Zr_{1-y}Mn_yO_2$), Å	Lattice parameter a of $ZrO_2{}^*$, Å
He	99% $Zr_{1-y}Mn_yO_2$; 1% MnO	190	5.064(1)
H_2/He	99% $Zr_{1-y}Mn_yO_2$; 1% MnO	200	5.065(1)
O_2/He	99% $Zr_{1-y}Mn_yO_2$; 1% Mn_2O_3	130	5.055(1)

In addition, in oxygen-containing atmosphere, the phase with the lowest CSR value is formed. Besides, small amount of manganese oxide (1 %) is present in all samples. In the case of inert and reducing environments, this is MnO, while in the oxidizing environment Mn_2O_3 oxide is formed. This is consistent with the TEM data, which showed the presence of a Mn_3O_4 phase in the sample Mn–Zr-400. Probably the presence of this phase became more obvious during heating, while the gas environment led to the reduction/oxidation of the precursor oxide. On the other hand, the presence of manganese oxide may indicate partial decomposition of the solid solution phase.

3.5. Thermogravimetric analysis

The TGA and DSC curves for the Mn–Zr-400 sample in He and in air are shown in Fig. 9a and Fig. 9b, respectively. The total weight loss from room temperature to 900 °C of is 9.7 and 10 %, respectively. The endothermic peak at 52 °C in He and at 65 °C in air corresponds to the removal of residual water and/or gases, which is accompanied by a weight loss of approximately 7 %. A very intense exothermic peak is observed at 645 °C in He (Fig. 9a) and 658 °C in air (Fig. 9b). In this case, this peak is likely to be due to the crystallization process [10, 30], which is also accompanied by rapid loss of a small amount of mass. In air, crystallization is shifted to the higher temperatures by approximately 13 °C, which indicates the influence of the environment on the process. Additionally, the heat release is more intense in air than in He (the maximum value is 0.27 μV/mg and 0.19 μV/mg, respectively). This extra heat release could be caused by

the oxidation of Mn cations in the solid solution phase or the oxidation of Mn_3O_4 oxide to Mn_2O_3, since the latter was detected by XRD analysis (Table 2). In the temperature range of approximately 700 – 900 °C, an endothermic behavior is observed, which indicates the instability of the formed phase [31]. This may be due to a further phase transformation of cubic/tetragonal zirconia to monoclinic modification which is typical for doped ZrO_2 [20, 32].

For comparison, a similar experiment was also carried out for the ZrO_2-300 sample in He (Fig. 9c) and in air (Fig. 9d). The total weight loss was approximately 12 % in both cases. At temperatures of 61 – 65 °C, a small endothermic peak is observed, which similarly to Mn–Zr-400 sample is associated with the removal of water and residual gases, which is also accompanied by a weight loss of approximately 3 – 4 %. At 425 °C, an exothermic peak is observed both in He and in air. In this case, this peak corresponds to the crystallization process with the formation of monoclinic ZrO_2, that is stable in this temperature range. Further heating leads to exothermic behavior. Probably this part of the curve may represent further phase transformation from monoclinic to tetragonal zirconia [6], which is not completed up to 900 °C.

Thus, a comparison of the TGA and DSC data of Mn–Zr-400 and ZrO_2-300 showed that the presence of the Mn dopant leads, firstly, to a shift in the crystallization temperature to the higher values, and, secondly, makes the crystallization process dependent on the gas environment.

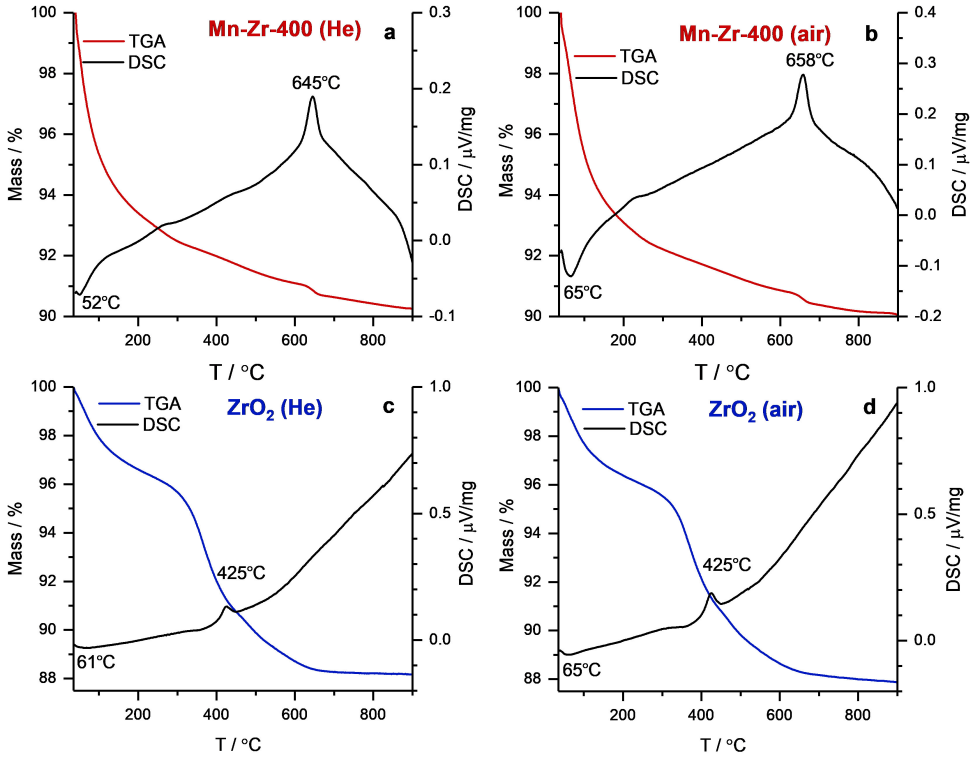

FIG. 9. TGA and DSC curves of Mn-Zr-400 sample in He (a) and in an air (b) and of ZrO_2-300 sample in He (c) and in an air (d)

4. Discussion

As it was shown in the in situ XRD experiments (Fig. 7–8), the process of crystallization is accompanied by the decrease in CSR of zirconia phase with temperature. Typically, the crystal growth implies the increase of the particle size and, consequently, of CSR. However, it is known that Mn–Zr solid solutions are characterized by a smaller particle size than pure zirconia [27]. In this case, we observe an average picture in the diffraction patterns, so CSR calculated from these patterns is also an average value. Therefore, the reduction of CSR upon heating may be due to an increase in the content of the phase of solid solution $Zr_{1-y}Mn_yO_2$ with a higher manganese content and smaller particle size. At the same time, the amount of ZrO_2 phase with larger particle size decreases. Furthermore, it can be assumed that the process of solid solution formation delays the particle growth. Thus, we observe a decrease in CSR from 200 – 290 Å to 120 – 190 Å with heating. According to the TEM and PDF data, the manganese oxide phase is present in the Mn–Zr-400 sample, which is also preserved in the sample synthesized at 700 °C. The exact content of this phase is unknown, since the corresponding peaks are absent in the XRD patterns. However, Mn atoms uniformly distributed among Zr atoms in the amorphous precursor apparently prevented the formation of a bulk phase of pure crystalline zirconia. At the same time, this probably led to the preferable formation of a solid solution phase $Zr_{1-y}Mn_yO_2$. In situ XRD data show that the lattice parameter of the formed crystalline phase decreases with increasing temperature. Since an increase in the

parameter usually occurs during heating, we associate this behavior with structural transformations inside the sample. In this case, similar to the observed CSR dependance, we observe the gradual decrease in the lattice parameter from 5.086(1) – 5.088(1) Å to 5.072(1) – 5.082(1) Å with heating. This result is associated with the formation of the solid solution $Zr_{1-y}Mn_yO_2$ with a smaller lattice parameter and simultaneous decrease in the content of ZrO_2 with a larger lattice parameter.

In papers [9–11] doping zirconia with vanadium, lanthanum and yttrium leads to the crystallization temperature increase. The authors explain this by the presence of admixture atoms (or oxide molecules) on the surface, which prevents grain growth, that results in a higher temperature to be required to initiate the crystallization process. In our case, the shift of the crystallization process to a higher temperature region seemed to prevent the formation of monoclinic ZrO_2 crystallites. Instead, the crystalline phase formed at temperatures of 460–560 °C has a cubic (or tetragonal) structure stabilized by manganese cations (Table 1). Previously [20], we showed that at the calcination temperature 800 °C, m-ZrO_2 was formed in similar coprecipitated Mn–Zr catalyst. This can be explained by the Mn-Zr solid solution decomposition resulting in the formation of pure undoped zirconia phase, for which the monoclinic modification is stable at 800 °C.

For Mn–Zr-400 sample the presence of Mn leads to the crystallization temperature being dependent on the environment. While in an inert and reducing environments the crystallization temperature, according to in situ XRD data, is 450 – 455 °C, in an oxidizing environment it is 560 °C. Moreover, TGA of ZrO_2-300 did not show a dependence of the crystallization temperature on the environment, unlike the manganese-containing catalyst, which is likely to be due to the redox properties of manganese. After treatment in an oxidizing environment, we also observed a smaller value of the lattice parameter of the solid solution $Zr_{1-y}Mn_yO_2$ than in the other two cases. This may indicate both a higher concentration of manganese cations in the solid solution and their partial oxidation.

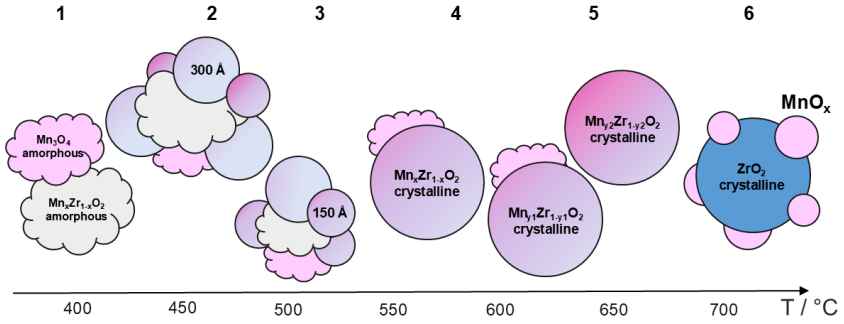

FIG. 10. Illustration of crystallization process: 1 – amorphous Mn-Zr mixed phase and oxide Mn_3O_4; 2 – thermally activated crystallization with the formation of large (300 Å) crystallites; 3 – formation of the solid solution phase $Mn_xZr_{1-x}O_2$; 4, 5 – crystallization finishes; 5, 6 – decomposition of solid solution with the formation of bulk manganese oxide phase.

The possible course of this process is shown schematically in Fig. 10. At 400 °C an amorphous phase containing uniformly distributed Zr and Mn atoms is present, as well as a small amount of Mn_3O_4 (1). At 460 – 560 °C the crystallization process starts, during which crystalline ZrO_2 phase is formed (2). Further heating leads to a decrease in the content of ZrO_2 phase with a larger particle size with simultaneous increase in the content of solid solution $Mn_yZr_{1-y}O_2$ with smaller particle size, which results in a decrease in the CSR from 200 – 290 to 120 – 190 Å (3). Crystallization is completed at 600 – 650 °C and the concentration of Mn atoms in the solid solution phase reaches its maximum (4 – 5). At 650 – 700 °C partial decomposition of the solid solution probably occurs with the formation of the bulk MnO_x phase (5 – 6).

5. Conclusion

The samples Mn–Zr-400 and Mn–Zr-700 were obtained by co-precipitation and calcination at the temperatures 400 and 700 °C, respectively. The sample ZrO_2-300 calcined at 300 °C was used as a reference. These samples were characterized by X-ray diffraction, pair distribution function analysis, BET and transmission electron microscopy. Mn–Zr-400 is shown to be amorphous and containing uniformly distributed Mn and Zr atoms, as well as a small amount of MnO_x phase. Mn–Zr-700 contains $Zr_{1-y}Mn_yO_2$ solid solution phase based on tetragonal zirconia and also shows traces of MnO_x phase. The sample ZrO_2-300 mainly consists of amorphous particles, but also shows the presence of crystalline zirconia phase unlike the sample Mn–Zr-400.

The process of crystallization was studied via in situ X-ray diffraction and thermogravimetric analysis. The crystallization temperature of Mn–Zr-400 in reducing and inert environments is 450 – 455 °C and in oxidizing is 560 °C. The crystallization of pure zirconia occurs at 425 °C in both oxidizing and inert environments. As the result of crystallization $Zr_{1-y}Mn_yO_2$ solid solution phase based on tetragonal modification. Further heating leads to an increase in the concentration of manganese in the solid solution (y), after which $Zr_{1-y}Mn_yO_2$ is stable up to 700 °C.

Thus, it was shown that the presence of manganese leads to the following effects:

– Shift of the crystallization onset to the higher temperatures compared to pure amorphous zirconia;
– The resulting phase of crystallization is the solid solution $Zr_{1-y}Mn_yO_2$ rather than pure ZrO_2.

Mn cations seem to stabilize the tetragonal modification of zirconia, while in this temperature range usually monoclinic zirconia is stable. Besides, the addition of manganese allows the crystallization temperature to be controlled by varying the environment. While the reducing environment apparently has no significant effect compared to the inert one, the oxidizing environment allowed the crystallization temperature to be increased.

Appendix

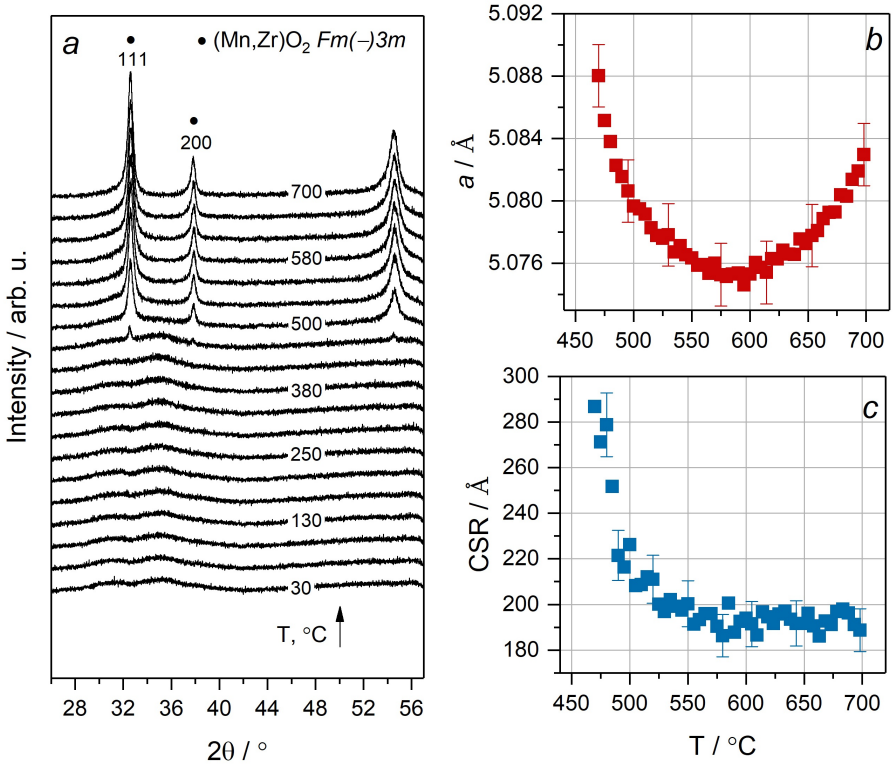

FIG. A1. XRD patterns of Mn–Zr-400 recorded upon heating from 30 to 700 °C with a rate of 5 °C/min in the H_2/He medium; $\lambda = 1.6467$ Å (a) change in the lattice parameter (b) and CSR (c) of $Zr_{1-y}MnyO_2$ with temperature

References

[1] Scotti N., Bossola F., Zaccheria F., Ravasio N. Copper–zirconia catalysts: Powerful multifunctional catalytic tools to approach sustainable processes. *Catalysts*, 2020, **10** (2), 168.
[2] Goscianska J., Ziolek M., Gibson E., Daturi M. Novel mesoporous zirconia-based catalysts for WGS reaction. *Appl. Catal. B Environ.*, 2010, **97**, P. 49–56.
[3] Liu J., Zhao Z., Xu C., Liu J. Structure, synthesis, and catalytic properties of nanosize cerium-zirconium-based solid solutions in environmental catalysis. *Chinese J. Catal.*, 2019, **40**, P. 1438–1487.
[4] Khurshid M., Al-Daous M. A., Hattori H., Al-Khattaf S.S. Effects of hydrogen on heptane isomerization over zirconium oxide modified with tungsten oxide and platinum. *Appl. Catal. A Gen.*, 2009, **362**, P. 75–81.
[5] Kumar A., Badoni R.P., Singhal S., Agarwal S., Tripathi A.R. Synthesis and characterization of zirconia-based catalyst for the isomerization of n-hexane. *Chem. Eng. Commun.*, 2017, **205** (1), P. 92–101.
[6] Howard C.J., Hill R.J., Reichert B.E. Structures of ZrO_2 polymorphs at room temperature by high-resolution neutron powder diffraction. *Acta Crystallogr.*, 1988, **B44**, P. 116–120.
[7] Yanwei Z., Fagherazzi G., Polizzi S. The local structure characterization and resulting phase-transition mechanism of amorphous ZrO_2. *J. Mater. Sci.*, 1995, **30**, P. 2153–2158.
[8] Tiseanu C., Parvulescu V.I., Cojocaru B., Pemartin K., Sanchez-Dominguez M., Boutonnet M. In situ Raman and time-resolved luminescence investigation of the local structure of ZrO_2 in the amorphous to crystalline phase transition. *J. Phys. Chem. C*, 2012, **116** (31), P. 16776–16783.
[9] Svoboda R., Bulánek R., Galusek D., Hadidimasouleh R., Ganjkhanlou Y. Crystal formation in vanadium-doped zirconia ceramics. *Cryst. Eng. Comm.*, 2018, **20**, P. 3105–3116.
[10] Sohn J.R., Cho S.G., Pae Y.Il., Hayashi S. Characterization of vanadium oxide-zirconia catalyst. *J. Catal.*, 1996, **159** (1), P. 170–177.
[11] Ushakov S.V., Brown C.E., Navrotsky A. Effect of La and Y on crystallization temperatures of hafnia and zirconia. *J. Mater. Res.*, 2004, **19**, P. 693–696.

[12] Afonasenko T.N., Bulavchenko O.A., Gulyaeva T.I., Tsybulya S.V., Tsyrul'nikov P.G. Effect of the Calcination Temperature and Composition of the MnO_x–ZrO_2 System on Its Structure and Catalytic Properties in a Reaction of Carbon Monoxide Oxidation. *Kinet. Catal.*, 2018, **59**, P. 104–111.
[13] Grabchenko M.V., Mamontov G.V., Chernykh M.V., Vodyankina O.V., Salaev M.A. Synergistic effect in ternary CeO_2-ZrO_2-MnO_x catalysts for CO oxidation and soot combustion. *Chem. Eng. Sci.*, 2024, **285**, 119593.
[14] Liberman E.Y., Kleusov B.S., Naumkin A.V. Thermal Stability and Catalytic Activity of the MnO_x–CeO_2 and the MnO_x–ZrO_2–CeO_2 Highly Dispersed Materials in the Carbon Monoxide Oxidation Reaction. *Inorg. Mater. Appl. Res.*, 2021, **12**, P. 468–476.
[15] López E.F., Escribano V.S., Resini C., Gasllardo-Amores J.M., Busca G. A study of coprecipitated Mn-Zr oxides and their behaviour as oxidation catalysts. *Appl. Catal. B Environ.*, 2001, **29**, P. 251–261.
[16] Qu Y., Zhu S., Zhang L. Low-temperature catalytic combustion of benzene over Zr–Mn mixed oxides synthesized by redox-precipitation method. *J. Mater. Sci.*, 2021, **56**, P. 13540–13555.
[17] Xu H., Yan N., Qu Z., Liu W., Mei J., Huang W., Zhao S. Gaseous Heterogeneous Catalytic Reactions over Mn-Based Oxides for Environmental Applications: A Critical Review. *Environ. Sci. Techno.*, 2017, **51** (16), P. 8879–8892.
[18] Koh D.J., Chung J.S., Kim Y.G., Lee J.S., Nam I., Moon S.H. Structure of MnZr mixed oxide catalysts and their catalytic properties in the CO hydrogenation reaction. *Journal of Catalysis.*, 1992, **138**, P. 630–639.
[19] Choudhary V.R., Uphade B.S., Pataskar S.G. Low temperature complete combustion of dilute methane over Mn-doped ZrO_2 catalysts: Factors influencing the reactivity of lattice oxygen and methane combustion activity of the catalyst. *Appl. Catal. A Gen.*, 2002, **227** (1–2), P. 29–41.
[20] Bulavchenko O.A., Konovalova V.P., Saraev A.A., Kremneva A.M., Rogov V.A., Gerasimov E.Y., Afonasenko T.N. The Catalytic Performance of CO Oxidation over MnO_x–ZrO_2 Catalysts: The Role of Synthetic Routes. *Catalysts.*, 2023, **13**, 57.
[21] Aulchenko V.M., Evdokov O.V., Kutovenko V.D., Pirogov B.Ya., Sharafutdinov M.R. One-coordinate X-ray detector OD-3M. *Nucl. Instruments Methods Phys. Res. Sect. A Accel. Spectrometers, Detect. Assoc. Equip.*, 2009, **603**, P. 76–79.
[22] Kabekkodu S.N., Dosen A., Blanton T.N. PDF–5+: A comprehensive powder diffraction file™ for materials characterization. *Powder Diffr.*, 2024, **39**, P. 47–59.
[23] Degen T., Sadki M., Bron E., König U., Nénert G. The high score suite. *Powder Diffraction.*, 2014, **29**, S13–S18.
[24] Patterson A.L. The Scherrer Formula for X-ray Particle Size Determination. *Phys. Rev.*, 1939, **56**, 978.
[25] Qiu X., Thompson J.W., Billinge S.J.L. PDFgetX2: A GUI-driven program to obtain the Pair Distribution Function from X-ray Powder Diffraction Data. *J. Appl. Cryst.*, 2004, **37**, 678.
[26] Farrow C.L., Juhas P., liu J.W., Bryndin D., Božin E.S. PDFfit2 and PDFgui: computer programs for studying nanostructure in crystals. *J. Phys. Condens. Matter.*, 2007, **19**, 33.
[27] Bulavchenko O.A., Vinokurov Z.S., Afonasenko T.N., Tsyrul P.G. Reduction of mixed Mn–Zr oxides: in situ XPS and XRD studies. *Dalt. Trans.*, 2015, **44**, P. 15499–15507.
[28] Shannon R.D. Revised effective ionic radii and systematic studies of interatomic distances in halides and chalcogenides. *Acta Crystallogr.*, 1976, **A32**, P. 751–767.
[29] Vanderbilt D., Zhao X., Ceresoli D. Structural and dielectric properties of crystalline and amorphous ZrO_2. *Thin Solid Films.*, 2005, **486**, P. 125–128.
[30] Aguilar D.H., Torres-Gonzalez L.C., Torres-Martinez L.M., Lopez T., Quintana P. A study of the crystallization of ZrO_2 in the sol-gel system: ZrO_2-SiO_2. *J. Solid State Chem.*, 2001, **158**, P. 349–357.
[31] Prasad K., Pinjari D.V., Pandit A.B., Mhaske S.T. Synthesis of zirconium dioxide by ultrasound assisted precipitation: Effect of calcination temperature. *Ultrason. Sonochem.*, 2011, **18**, P. 1128–1137.
[32] Afonasenko T.N., Glyzdova D.V., Yurpalov V.L., Konovalova V.P., Rogov V.A., Gerasimov E.Y., Bulavchenko O.A. The Study of Thermal Stability of Mn–Zr–Ce, Mn–Ce and Mn-Zr Oxide Catalysts for CO Oxidation. *Materials.*, 2022, **15** (21), 7553.

Submitted 29 April 2025; revised 1 December 2025; accepted 12 December 2025

Information about the authors:

Valeria P. Konovalova – Boreskov Institute of Catalysis SB RAS, Lavrentiev Ave, 5, Novosibirsk, 630090, Russia; ORCID 0000-0003-4101-599X; lekorux@gmail.com

Evgeny Yu. Gerasimov – Boreskov Institute of Catalysis SB RAS, Lavrentiev Ave, 5, Novosibirsk, 630090, Russia; ORCID 0000-0002-3230-3335; gerasimov@catalysis.ru

Zahar S. Vinokurov – Synchrotron Radiation Facility SKIF, Nikol'sky Prospekt, 1, Kol'tsovo, 630559, Russia; ORCID 0000-0002-2737-098X; vinzux@mail.ru

Alena A. Pochtar – Boreskov Institute of Catalysis SB RAS, Lavrentiev Ave, 5, Novosibirsk, 630090, Russia; ORCID 0000-0001-7607-2025; po4tar@catalysis.ru

Olga A. Bulavchenko – Boreskov Institute of Catalysis SB RAS, Lavrentiev Ave, 5, Novosibirsk, 630090, Russia; Synchrotron Radiation Facility SKIF, Nikol'sky Prospekt, 1, Kol'tsovo, 630559, Russia; ORCID 0000-0001-5944-2629; obulavchenko@catalysis.ru

Conflict of interest: the authors declare no conflict of interest.